Vagus nerve modulates acute-on-chronic liver failure progression via CXCL9

Li Wu[1,2,3], Jie Li[1,2,3], Ju Zou[1,2,3], Daolin Tang[4], Ruochan Chen[1,2,3]

[1]Hunan Key Laboratory of Viral Hepatitis, Xiangya Hospital, Central South University, Changsha, Hunan 410008, China;
[2]Department of Infectious Diseases, Xiangya Hospital, Central South University, Changsha, Hunan 410008, China;
[3]National Clinical Research Center for Geriatric Disorders, Xiangya Hospital, Central South University, Changsha, Hunan 410008, China;
[4]Department of Surgery, UT Southwestern Medical Center, Dallas, TX, USA.

Abstract

Background: Hepatic inflammatory cell accumulation and the subsequent systematic inflammation drive acute-on-chronic liver failure (ACLF) development. Previous studies showed that the vagus nerve exerts anti-inflammatory activity in many inflammatory diseases. Here, we aimed to identify the key molecule mediating the inflammatory process in ACLF and reveal the neuroimmune communication arising from the vagus nerve and immunological disorders of ACLF.

Methods: Proteomic analysis was performed and validated in ACLF model mice or patients, and intervention animal experiments were conducted using neutralizing antibodies. PNU-282987 (acetylcholine receptor agonist) and vagotomy were applied for perturbing vagus nerve activity. Single-cell RNA sequencing (scRNA-seq), flow cytometry, immunohistochemical and immunofluorescence staining, and clustered regularly interspaced short palindromic repeats/CRISPR-associated protein 9 (CRISPR/Cas9) technology were used for *in vivo* or *in vitro* mechanistic studies.

Results: The unbiased proteomics identified C-X-C motif chemokine ligand 9 (CXCL9) as the greatest differential protein in the livers of mice with ACLF and its relation to the systematic inflammation and mortality were confirmed in patients with ACLF. Interventions on CXCL9 and its receptor C-X-C chemokine receptor 3 (CXCR3) improved liver injury and decreased mortality of ACLF mice, which were related to the suppressing of hepatic immune cells' accumulation and activation. Vagus nerve stimulation attenuated while vagotomy aggravated the expression of CXCL9 and the severity of ACLF. Blocking CXCL9 and CXCR3 ameliorated liver inflammation and increased ACLF-associated mortality in ACLF mice with vagotomy. scRNA-seq revealed that hepatic macrophages served as the major source of CXCL9 in ACLF and were validated by immunofluorescence staining and flow cytometry analysis. Notably, the expression of CXCL9 in macrophages was modulated by vagus nerve-mediated cholinergic signaling.

Conclusions: Our novel findings highlighted that the neuroimmune communication of the vagus nerve–macrophage–CXCL9 axis contributed to ACLF development. These results provided evidence for neuromodulation as a promising approach for preventing and treating ACLF.

Keywords: Acute-on-chronic liver failure; CXCL9; Vagus nerve; Neuroimmune communication; ACLF

Introduction

Acute-on-chronic liver failure (ACLF) is a clinical syndrome manifesting as acute and severe hepatic derangements.[1] As the major cause of death in patients with chronic liver disease (CLD) like cirrhosis worldwide, ACLF is characterized by multiorgan failures and high rates of short-term mortality.[2] Currently, there are no specific treatments for ACLF and liver transplantation is considered the only curative treatment for ACLF.[2] Unfortunately, due to the shortage of organ donors, high expenses, and recurrent contraindications, only a few patients can receive liver transplantation.[3] Therefore, exploring the key pathophysiological mechanism leading to the development and progression of ACLF is an urgent need to improve the clinical prognosis of patients.

Systemic inflammation is the primary driver for ACLF leading to major complications and organ failures.[4] Therapeutic approaches including liver support systems and albumin administration were used to mitigate the severe systemic inflammation in ACLF. However, their effects are controversial.[5] The hepatic accumulation of inflammatory cells is generally greater in ACLF than in other CLDs, which caused the subsequent systemic inflammation.[3]

Access this article online

Quick Response Code:

Website: www.cmj.org

DOI: 10.1097/CM9.0000000000003104

Li Wu and Jie Li contributed equally to this work.

Correspondence to: Ruochan Chen, Key Laboratory of Viral Hepatitis of Hunan Province, Xiangya Hospital, Central South University, No. 87 Xiangya Road, Kaifu District, Changsha, Hunan 410008, China
E-Mail: 405031@csu.edu.cn

Copyright © 2024 The Chinese Medical Association, produced by Wolters Kluwer, Inc. under the CC-BY-NC-ND license. This is an open access article distributed under the terms of the Creative Commons Attribution-Non Commercial-No Derivatives License 4.0 (CCBY-NC-ND), where it is permissible to download and share the work provided it is properly cited. The work cannot be changed in any way or used commercially without permission from the journal.

Chinese Medical Journal 2025;138(9)
Received: 21-02-2024; **Online:** 28-06-2024 **Edited by:** Yanjie Yin

Given the lack of specific treatment strategies to address the complex systemic inflammation in ACLF, identify the pathophysiological mechanisms mediating ACLF-associated hepatic inflammation is promising for exploring therapeutic targets.

Accumulating evidence indicates that neuronal circuits are organized in a reflexive manner to innervate immune responses.[6] Especially, the vagus nerve, which parasympathetically stimulates visceral organs,[7] mediates cholinergic signaling to regulate inflammation via α7 nicotinic acetylcholine receptor (AChR) in immune cells.[6,8] Previous studies regarding endotoxins,[9] ischemia-reperfusion injury,[10] and pancreatitis[11] have reported that the cholinergic regulation of the vagus nerve was involved in many inflammatory responses. Thus, molecular insights into neuroimmune interactions are promising to identify therapeutic targets for inflammatory diseases. Neuromodulation in the liver by the vagus nerve depends on acetylcholine (ACh), as evidenced by the fact that AChR-knockout mice mimicked the effects of hepatic vagotomy.[12] Despite previous studies reported that the vagus nerve regulates basic physiological and metabolic functions of the liver,[13,14] the neuroimmune interaction between the vagus nerve and the immune response associated with ACLF progression remains unclear.

In the present study, we aimed to identify the key molecule mediating the hepatic inflammation in ACLF and reveal the neuroimmune communication to explore novel strategies for managing ACLF-associated hepatic immunological disorders.

Methods

Mouse models

The animal experiments were approved by the Institutional Animal Care and Use Committee of the Xiangya Hospital (No. 2019030151). All animal experiments took place in the Department of Laboratory Animals, Central South University. Mice were housed in polycarbonate cages (four mice per cage) and maintained in a temperature- and light-controlled facility (12 h:12 h light–dark cycle) with *ad libitum* access to standard food and water.

According to a previous publication, we constructed the ACLF mouse model in a three-stage manner with slight modifications.[15] The first stage was the "chronic liver injury stage" in which 8-week-old male C57BL/6J mice were injected intraperitoneally (i.p.) with CCl_4 (0.2 mL/kg, twice a week) for 12 weeks. And assessment was carried out by Masson and hematoxylin and eosin (H&E) staining to determine liver fibrosis. The second stage was the "acute insult stage" in which the mice were administered a double dose of CCl_4 (0.4 mL/kg) to cause acute liver injury. The third stage was the "lipopolysaccharide (LPS) challenge stage" to mimic the bacterial infection common in patients with ACLF in which we challenged the mice with LPS (5 mg/kg, i.p.). Mortality, alanine aminotransferase (ALT) levels, and pathological examination of the liver were used to determine whether the mice models were optimal for the experiment. Mice were intraperitoneally treated with anti-CXCL9 antibody (4.5 mg/kg) (Bioxcell, West Lebanon, NH, USA), anti-C-X-C chemokine receptor 3 (CXCR3) (250 μg/mouse) (Bioxcell), or their isotype immunoglobulin G2 (IgG2) control (0.5 mg/kg) (BioLegend, San Diego, CA, USA), or PNU-282987 (a specific α7 nicotinic AChR agonist) (3 mg/kg, Beyotime Biotechnology, Shanghai, China) at an established dose according to previous publications.[16,17] The selective hepatic vagotomy was performed following a previous study.[18] Briefly, all the mice were anesthetized by an intraperitoneal injection of sodium pentobarbital (50 mg/kg weight; Dainippon Pharmaceutical Co., Osaka, Japan). The abdomen was incised along the midline by scissors and kept open by retractors. After the intestines were displaced to the outside of the lower abdomen, the hepatic branch, which leaves the anterior vagal trunk a few millimeters below the diaphragm, was exposed and completely transected. Thereafter, the intestines were returned and the abdominal cavity was closed with ophthalmologic sutures in two layers. The procedure was carried out with minimal blood loss and took approximately 10–15 min.

Human samples

This human study was conducted in accordance with the *Declaration of Helsinki* 1975 as revised in 2000 and the procedures were approved by the Ethics Committee of the Xiangya Hospital, Central South University (No. 2019030151). The study subjects were informed the purpose of the study and informed consents were obtained. Serum samples from patients with ACLF (n = 162; 76 survivors and 86 non-survivors at day 90 after the diagnosis) and CLD (n = 23). The characteristics of the study subjects are described in Supplementary Table 1, http://links.lww.com/CM9/B975. The formalin-fixed liver tissues from patients with ACLF (n = 3) who underwent liver transplantation and patients with CLD (n = 3) who underwent diagnostic liver biopsy were obtained from the Departments of Pathology of Xiangya Hospital, Central South University. Regarding that our patients were all from Asian countries, ACLF was diagnosed according to the Asian Pacific Association for the Study of the Liver (APASL) criteria.[19]

Proteomics analysis

Chemical reagents

High performance liquid chromatography (HPLC) grade acetonitrile, water, BCA Protein Assay Kit, and tandem mass tag (TMT) label reagent were purchased from Thermo Fisher Scientific (Waltham, MA, USA). Protease inhibitor was purchased from AMRESCO Inc. (Solon, OH, USA). Iodoacetamide, trypsin, and dithiothreitol were purchased from Sangon Biotech (Shanghai, China).

Sample preparation

Frozen liver samples were lysed with 300 μL digestion buffer supplemented with 1 mmol/L protease inhibitor on a homogenizer. The samples were centrifuged (12,000 ×g for 10 min) and insoluble particles were removed after sonication. Then, the supernatant was obtained and the

protein concentration was measured using BCA Protein Assay Kit. Next, 100 μg of protein was reduced and digested by dithiothreitol, iodoacetamide, and trypsin.[20] The protein precipitation was acquired after centrifugation (12,000 ×g for 20 min) and vacuum freeze-dried, and labeled with TMT label reagent.

Liquid chromatography-mass spectrometry

Peptide separation was performed on an 1100 HPLC System (Agilent Technologies, Foster City, CA, USA) equipped with the Agilent Zorbax Extend reverse phase (RP) column (5 μm, 150 mm × 2.1 mm) and monitored at 210 nm and 280 nm. The eluents employed were 2–98% gradient of acetonitrile in HPLC water in 75 min. Dried samples were collected from 8 min to 60 min and elution buffer was collected in every minute and numbered from 1 to 15, and then lyophilized for mass spectrometry detection. The Q-Exactive HF mass spectrometer (Thermo Fisher Scientific) equipped with a Nanospray Flex source (Thermo Fisher Scientific) was used for mass spectrometry analysis and data were acquired by a full mass spectrometry (MS) (range 300–1600 m/z) followed by data-dependent MS/MS scans.

Bioinformatics analysis

Raw data were processed in Proteome Discoverer (v.2.2) to search against the protein database with trypsin digestion specificity. For the protein quantification method, TMT 6-plex was selected. Proteins and peptides with a fold discovery rate <0.01 were retained for further identification. If the fold change (FC) was greater than 1.5 or less than 2/3 and the *P*-value was less than 0.05, it was considered to be a differentially expressed proteins (DEPs). And then functional analysis of DEPs was performed by referring to Gene Ontology (GO) and Kyoto Encyclopedia of Genes and Genomes (KEGG) databases using the OmicsBean cloud platform.

Hematological examination

Ethylene diaminetetra acetic acid (EDTA) anti-coagulated blood samples were collected from the patients. Hematological examinations were performed using a Hemavet 950 FS Hematology Analyzer (Drew Scientific, Dallas, TX, USA).

Measurement of CXCL19 by enzyme-linked immunosorbent assay (ELISA)

The blood samples from patients were collected and centrifugation (3500 r/min, 15 min) to obtain serum. Then the serum levels of CXCL9 were measured using ELISA kit (R&D Systems, Minneapolis, MN, USA) according to the manufacturer's procedure. And samples were read at 450 nm by PerkinElmer Multimode Plate Readers (PerkinElmer Inc., Waltham, Massachusetts, USA).

Liver injury and fibrosis analysis

Formalin-fixed and paraffin-embedded liver tissues were stained with H&E on 4 μm-thick sections for histological evaluation. ALT levels were detected using a Catalyst Dx Chemistry Analyzer with ALT chips (IDEXX Laboratories, Westbrook, ME, USA). Liver injury and fibrosis were assessed via H&E staining. And the commonly used Ishak scoring system was assessed by two independent pathologists to comprehensively take necrosis, apoptosis, and portal inflammation into consideration. The areas were randomly selected and evaluated for histological signs of hepatocyte necrosis and apoptosis, immune cell infiltration, and fibrosis.

Immunohistochemistry and immunofluorescence staining

Paraffin-embedded liver tissues were cut into 4 μm sections for immunohistochemistry or immunofluorescence staining. Immunohistochemistry staining was performed with anti-CXCL9 antibody (Servicebio, Wuhan, China), and then stained brown by diaminobenzidine (DAB). Immunofluorescence staining was conducted with antibodies of CXCL9 (Servicebio), CXCR3 (Proteintech Group, Chicago, IL, USA), F4/80 (Cell Signaling Technology, Boston, MA, USA), cluster of differentiation 8 (CD)8 (Abcam, Cambridge, UK), CD206 (Abcam), and inducible nitric oxide synthase (iNOS) (Abcam). After incubation with the primary and secondary antibodies, tyramide signal amplification (TSA)-520 and TSA-690 (Abiowell, Changsha, China) were used for staining.

Flow cytometry analysis

Twelve hours post-treatment, mouse liver tissues were excised and digested post-mortem using a cocktail of 1640 medium, 5% fetal bovine serum, 0.5 mg/mL collagenase type IV (Sigma-Aldrich, St. Louis, MO, USA), and 0.1 mg/mL DNase I (Roche, Penzberg, Germany). After digestion at 37°C for 30 min, the cells were passed through a 70-μm filter twice. The cells were then analyzed using flow cytometry (BD Biosciences, San Jose, CA, USA)). In brief, flow cytometry and cell fluorescence measurements were performed using a BD Cantos II flow cytometer (BD Biosciences) and analyzed with FlowJo software (version 10.0.6; Tree Star, Ashland, OR, USA). The samples were analyzed for 100,000 events based on the immune cell population. The parameters for forward and side scatter (FSC/SSC) measurements were set to include all cell types potentially present in liver cell isolation and elutriation fractions (i.e., macrophages, neutrophils, $CD4^+$ T cells, $CD8^+$ T cells, natural killer (NK) cells, natural killer T (NKT) cells, γδ T cells, and $CD45^+F4/80^+iNOS^{+/}CD206^{+/-}$ cells). Populations were first interpreted using relative cell size and complexity in FSCs/SSCs, viability, and the presence or absence of cellular markers. The percentage of each cell type was calculated based on live cell populations, as determined by viability analysis.

For detection of interferon (IFN)-γ and Interleukin (IL)-17A production by immune cells, cells were cultured for 3 h with 10 ng/mL propidium monoazide (PMA) and 1 μg/mL ionomycin in the presence of Golgi Plug (BD Biosciences) and Golgi Stop (BD Biosciences). After 3 h, the cells were analyzed using flow cytometry. To detect

CXCL9, cells were cultured for 3 h in Golgi Plug/Stop in the absence of PMA/ionomycin.

Single-cell RNA sequencing (scRNA-seq)

Liver cells were prepared according to Single Cell 3′ Protocol and single liver cells (CLD, 8738 and ACLF, 6565) were obtained for the encapsulation. The cDNA libraries were sequenced with the NovaSeq 6000 System (Illumina Inc., San Diego, CA, USA). The raw data were processed using Cell Ranger software v6.0 (http://support.10xgenomics.com/single-cell/software/overview/welcome) for sequencing quality analysis and assessment. Seurat v4.0 (https://satijalab.org/seurat/) was used for cell clustering and was visualized by uniform manifold approximation and projection (UMAP). Each cluster with marker genes was identified by the FindAllMarkers function in Seurat and defined by a published article based on the top genes. Then, differentially expressed genes (DEGs) analysis and pathway enrichment analysis were performed using the OmicStudio tools created by LC-BIO Co., Ltd. (Hangzhou, China) at https://www.omicstudio.cn/cell and Shanghai NewCore Biotechnology Co., Ltd. (https://www.bioinformatics.com.cn, Last accessed on 2023 August 10).

Quantitative reverse-transcription polymerase chain reaction (qRT-PCR) analysis

Total RNA extraction with TRIzol Reagent (Invitrogen, Carlsbad, CA, USA) was performed according to the manufacturer's instructions, followed by cDNA synthesis using the High-Capacity cDNA Reverse Transcription Kit (Applied Systems, Foster City, CA, USA) and subjected to real-time PCR analysis of gene expression using the Quant Studio 6 Flex Real-time PCR system (Applied Biosystems, Foster City, CA, USA) in duplicate for each sample. The reaction mixture contained 3 μL cDNA (equal to 50 ng RNA), 0.5 μmol/L forward and reverse primers, and 10 μmol/L SYBR Green Master Mix (Abm, Vancouver, Canada) adjusted to a total of 20 μL. Amplification was performed at 50°C for 2 min, 95°C for 10 min, followed by 40 cycles at 95°C for 15 s and 60°C for 1 min, and followed by melting curve profiling to confirm specificity. Target gene expression levels were normalized to glyceraldehyde-3-phosphate dehydrogenase (GAPDH), followed by the comparative cycle threshold Ct method ($2^{-\Delta\Delta Ct}$). The primer sequences are summarized in Supplementary Table 2, http://links.lww.com/CM9/B975.

CRISPR knockout cell line generation

To generate knockout cell lines, 37 pmol single-guide RNA (sgRNA) (SyntheGo, Redwood City, CA, USA) and 270 pmol recombinant Cas9[21] were incubated together for 10 min at around 25°C. sgRNA/Cas9 ribonucleoprotein particles (RNPs) were then electroporated into target cells (3×10^5) using a Lonza SG Cell line kit and 4D-Nucleofector. Gene knockout was confirmed 48 h later using RT-PCR analysis. Two sgRNAs were used for each gene. The sequences used were as follows: CXCL9 g1: AUUUGUAGUGGAUCGUGCCU and g2: AACCUGCCUAGAUCCGGACU.

In vitro inflammation model

Donor-matched hepatocytes (H) and Kupffer cells (KCs) were co-isolated from individual mice using differential, density gradient, and counterflow elutriation centrifugation methods in established research.[22] We followed the procedures established by Rose *et al*[22] and made some changes accordingly to set up a hepatocyte and Kupffer cell co-culture (HKCC) system using a Transwell chamber HKCCs were plated at a 2:1 (H:K) ratio onto the upper and lower chambers of the Transwell system. After a 24-h acclimation period, the KCs were exposed to LPS (1 mg/mL) for 48 h. Hepatocyte inflammation was assessed by measuring ALT production in the culture medium after 48 h of LPS stimulation.

Statistical analysis

Statistical differences between groups were analyzed using one-way analysis of variance (ANOVA), two-way ANOVA, or Student's *t*-test as appropriate. The Kruskal–Wallis test was used for non-parametric variables. The Mantel–Cox log-rank test was used for survival comparison. *P*-values were calculated and significance was set at $P < 0.05$.

Results

Proteomic profiling linked unregulated CXCL9 to ACLF development

To identify the proteomic signature driving the progression of ACLF, high-throughput proteomics analysis was performed to identify the differential protein profiles in the liver samples between mice with ACLF and those with CLD. Totally, 4960 credible proteins were identified in the TMT-labeled proteomics experiments. Using a false discovery rate (FDR) filter with a *P*-value <0.05 and an FC >1.5-fold or <2/3-fold, we identified 167 DEPs between the mice with ACLF and CLD [Supplementary Figure 1A, http://links.lww.com/CM9/B975]. Furthermore, the unsupervised clustering heat map constructed based on these 167 DEPs could distinguish ACLF from CLD [Supplementary Figure 1B, http://links.lww.com/CM9/B975].

The GO enrichment analyses revealed that the biological processes of DEPs were mainly involved in defense responses, immune system processes, and responses to cytokines, organisms, and external stimuli [Supplementary Figure 1C, http://links.lww.com/CM9/B975]. The cellular components of DEPs were primarily related to the extracellular region, extracellular space, and membrane-bound vesicles [Supplementary Figure 1C, http://links.lww.com/CM9/B975]. In terms of molecular functions, the DEPs were mainly correlated with hydrolase activity, anion and ion bindings, and catalytic activity [Supplementary Figure 1C, http://links.lww.com/CM9/B975]. Pathway analysis revealed that the DEPs were mainly enriched in inflammatory pathways, including tumor necrosis factor (TNF) and nuclear factor-kappa B (NF-κB) signaling pathway, the renin–angiotensin system, complement and coagulation system, leukocyte transendothelial

migration, and infections of tuberculosis, *Staphylococcus aureus*, malaria, amoebiasis, and African trypanosomiasis [Supplementary Figure 1D, http://links.lww.com/CM9/B975]. Moreover, the DEPs were related to the metabolism of porphyrin, chlorophyll, nitrogen, amino acids, and lipids [Supplementary Figure 1D, http://links.lww.com/CM9/B975].

To explore the key biological molecules determining the development of ACLF, the top 10 DEPs between ACLF and CLD were obtained. As presented in Supplementary Figure 1E and Supplementary Table 3, http://links.lww.com/CM9/B975, all these 10 proteins were upregulated in the liver of mice with ACLF compared with CLD. Of note, CXCL9 showed the highest log_2FC value. Consistently, the qRT-PCR results revealed that the hepatic *CXCL9* gene expression was remarkably increased in mice with ACLF [Supplementary Figure 1F, http://links.lww.com/CM9/B975]. These findings suggested that DEPs, especially the upregulated CXCL9, might be involved in the pathogenesis of ACLF.

Increased CXCL9 expression related to systemic inflammation and mortality of ACLF patients

Due to the markedly different CXCL9 expression between mice with ACLF and CLD, we further examined the CXCL9 levels in ACLF patients. As shown in Figure 1A, the serum CXCL9 levels increased significantly in ACLF survivors compared to those in the CLD patients, and further increased in the ACLF non-survivors. Then, the ACLF patients were classified into high- and low-CXCL9 expression groups according to the median value of CXCL9. And the Kaplan–Meier curves showed significantly higher mortality of ACLF patients with high CXCL9 levels compared to those with low CXCL9 levels [Figure 1B]. Moreover, correlation analysis revealed that the CXCL9 levels were positively associated with C-reactive protein and circulating inflammatory cytokines, including TNF-α, IL-6, and IL-8 [Figure 1C–F]. Importantly, when analyzing the serum levels of other chemokines, including CCL2, CCL5, CXCL4, CXCL7, CXCL12, CCL20, CXCL10, and CXCL11, no significant difference was observed between the survivors and non-survivors of ACLF [Figure 1G]. These clinical observations suggested that CXCL9 was involved in the progression of ACLF.

Inhibition of CXCL9 and its receptor CXCR3 alleviated liver inflammation and decreased the mortality of ACLF model mice

To demonstrate the critical role of CXCL9 in ACLF development, we constructed a three-stage ACLF mouse model, as previously described[15] and neutralizing antibodies were used to block CXCL9 and its receptor CXCR3 [Figure 2A]. As shown in Supplementary Figure 2, http://links.lww.com/CM9/B975, the mice model mimicking the clinical course of ACLF was successfully built as presented by the results of the mortality, H&E staining of liver tissues, and ALT levels. The blockage of CXCL9 and CXCR3 markedly reduced the mortality rate of mice with ACLF compared to mice treated with immunoglobulin G (IgG) [Figure 2A]. Furthermore, mice treated with anti-CXCL9 or anti-CXCR3 antibodies showed a significant decrease in serum ALT levels at 36 h, 48 h, and 60 h post-CCl_4 injection compared to mice treated with IgG [Figure 2B]. Additionally, the H&E staining also showed that anti-CXCL9 or anti-CXCR3 treatment ameliorated liver injury including hepatocyte necrosis and inflammation [Figure 2C, D]. The improved Ishak scores strongly indicated that the blockage of

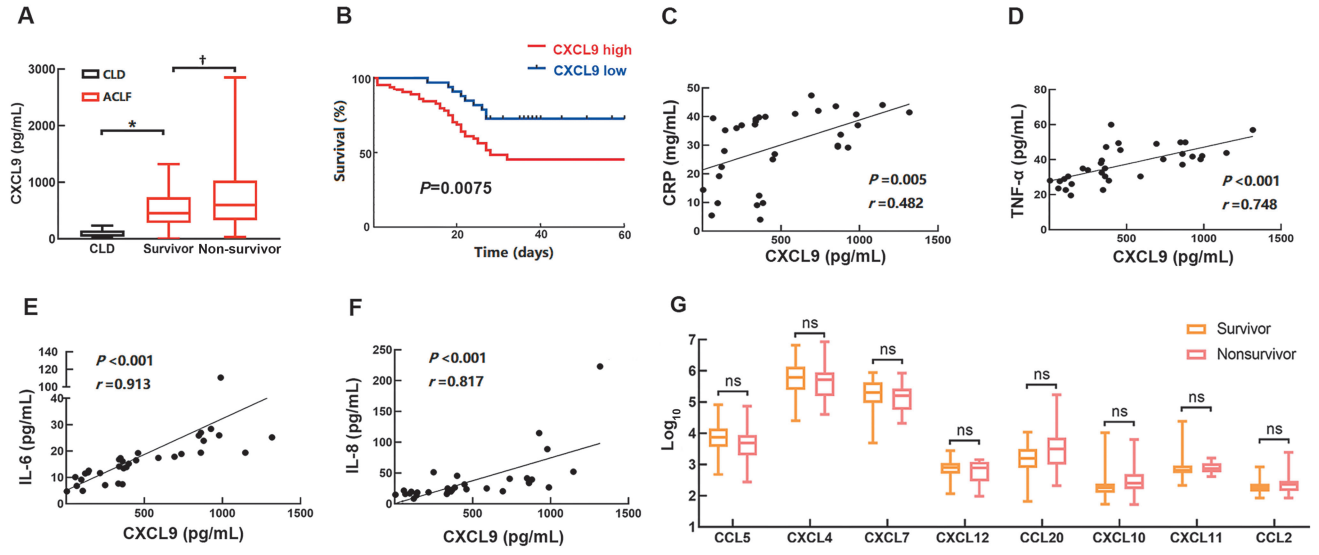

Figure 1: CXCL9 related to systemic inflammation and prognosis of ACLF patients. (A) Serum levels of CXCL9 in CLD patients and ACLF patients with different clinical outcomes. (B) Kaplan–Meier curves exhibited the overall survival of ACLF patients with high and low expression of CXCL9 who were classified according to the median of CXCL9 levels. (C–F) Correlation analysis between serum CXCL9 levels and indicators of systemic inflammation in ACLF patients was performed using Spearman's rank correlation analysis. (G) Comparison of the serum chemokines concentrations except CXCL9 between the survivors and non-survivors of ACLF patients. Data were given as median with range and *P*-values were calculated using Kruskal–Wallis test for three groups and Mann–Whitney *U* test or Student's *t*-test for two groups. $^{*}P<0.01$; $^{\dagger}P<0.001$. ACLF: Acute-on-chronic liver failure; CLD: Chronic liver disease; CXCL9: C-X-C motif chemokine ligand 9; IL: Interleukin; ns: Not significant; TNF: Tumor necrosis factor; OS: overall survival.

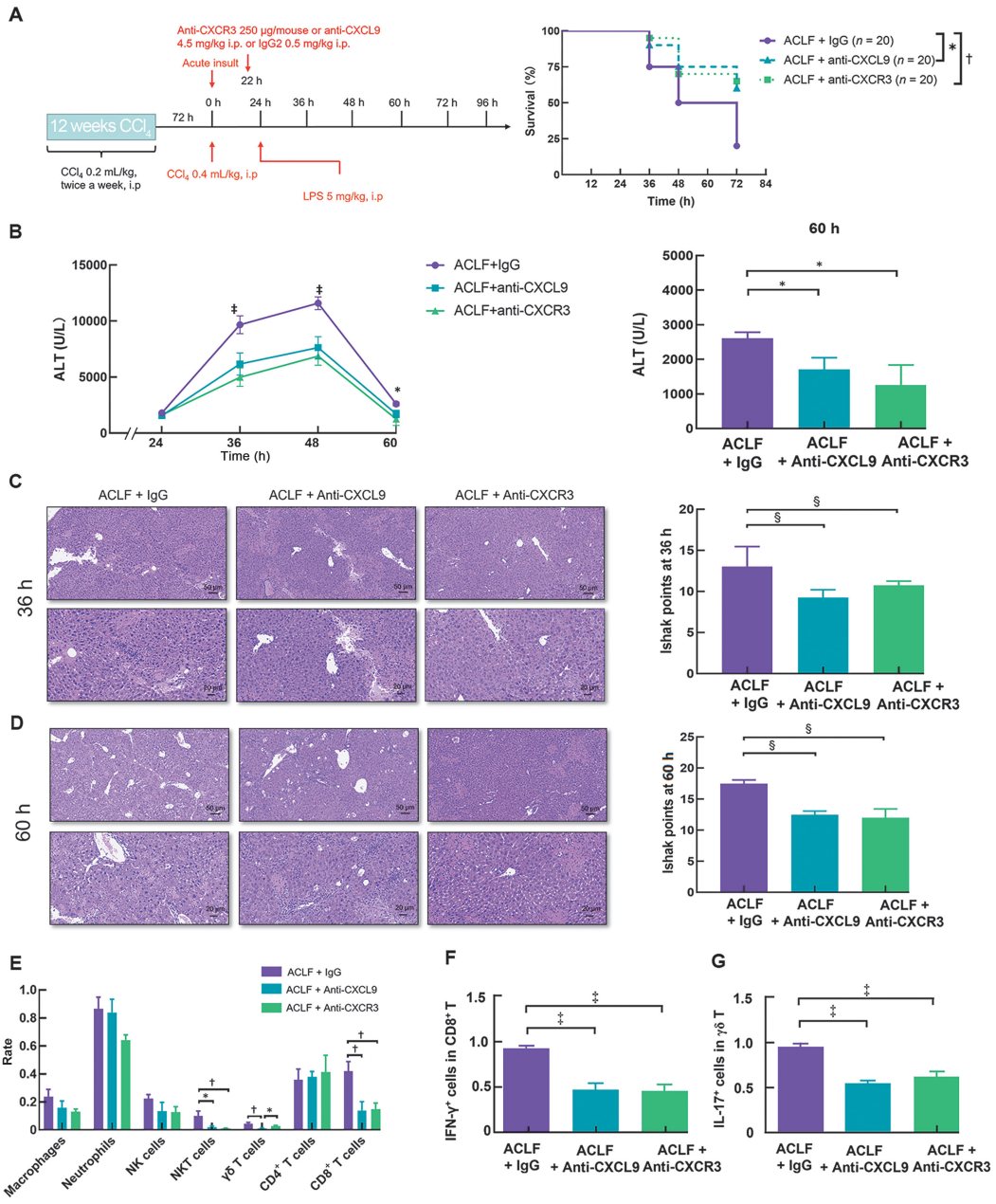

Figure 2: Inhibition of CXCL9 and its receptor CXCR3 alleviated liver injury and decreased mortality in the ACLF model. (A) Schematic timeline of the procedures. Mice were treated with 12-week CCl_4 to induce chronic liver injury followed by additional challenge with an acute insult (a double dose of CCl_4 injection) and then mice were injected with LPS. Anti-CXCR3, anti-CXCL9, or IgG was applied two hours before LPS injection. Survival rates were determined and Mantel–Cox log-rank tests were used for statistical analysis ($n = 20$ per group). (B) Serum ALT levels were measured every 12 h post-acute insult. The comparison of ALT among mice treated with anti-CXCR3, anti-CXCL9, and IgG at 60 h post-acute insult was shown. (C) Representative H&E staining images. (D) Comparison of Ishak points among three groups of mice. (E) Flow cytometry analysis of hepatic immune cell subsets including innate immune cells (macrophage, neutrophil, NK, NKT, and γδ T cells) and adaptive immune cells ($CD4^+$ T and $CD8^+$ T cells). (F, G) The percentage of IFN-γ-expressing $CD8^+$ T cells and IL-17A-expressing γδ T cells in the liver were analyzed by flow cytometry. Data were given as median with range or mean with SD and *P*-values were calculated using one-way analysis of variance or Kruskal–Wallis test. $^*P < 0.05$; $^\dagger P < 0.01$; $^\ddagger P < 0.001$; $^\S P < 0.0001$. ACLF: Acute-on-chronic liver failure; ALT: Alanine aminotransferase; CXCL9: C-X-C motif chemokine ligand 9; CXCR3: C-X-C chemokine receptor 3; H&E: Hematoxylin & eosin; IFN: Interferon; IgG: Immunoglobulin G; IL:Interleukin; LPS: Lipopolysaccharide; NKT: Natural killer T (cells); SD: Standard deviation.

CXCL9 and CXCR3 attenuated liver fibrosis in mice with ACLF [Figure 2C, D].

Hepatic accumulation of inflammatory cells is the driving force for ACLF progression. Thus, we studied the influence of CXCL9 on hepatic immune cell subsets using flow cytometry analysis. As shown in Figure 2E, the blockade of CXCL9 and its CXCR3 receptor significantly decreased the numbers of $CD8^+$ T cells, γδ T cells, and NKT cells in the livers of mice with ACLF, while showing no impact on the numbers of $CD4^+$ T cells, NK cells, neutrophils, and macrophages. In addition to a large decrease in immune cell numbers, the ratio of $CD8^+$ T cells expressing IFN-γ and γδ T cells expressing interleukin-17 (IL-17) was also decreased in ACLF mice which were treated with anti-CXCL9 or anti-CXCR3 antibodies, compared to those with IgG [Figure 2F, G]. Taken together, these findings evidenced that CXCL9 contributed to ACLF development and inhibition of the CXCL9/CXCR3

axis suppressed the accumulation and activation of immune cells and prevented ACLF progression.

Vagus nerve-regulated CXCL9 secretion in the pathogenesis of ACLF

Since the nervous system especially the vagus nerve controls chemokine production,[23] we further explored whether CXCL9 in ACLF was regulated by the vagus nerve. As shown in Figure 3A, B, mice with ACLF were either supplemented with the AChR agonist PNU-282987 or subjected to vagotomy to study the physiologic role of the vagus nerve. The survival curves showed that cholinergic elicitation by PNU-282987 decreased the mortality, while vagus nerve denervation through vagotomy significantly accelerated the death of mice with ACLF [Figure 3A, B]. The H&E staining showed an increased degree of hepatocyte necrosis and inflammation in the livers from vagotomized mice with ACLF compared to sham-operated mice or mice with saline, and these effects were attenuated by PNU-282987 supplementation [Figure 3C]. The significant difference in Ishak scores and

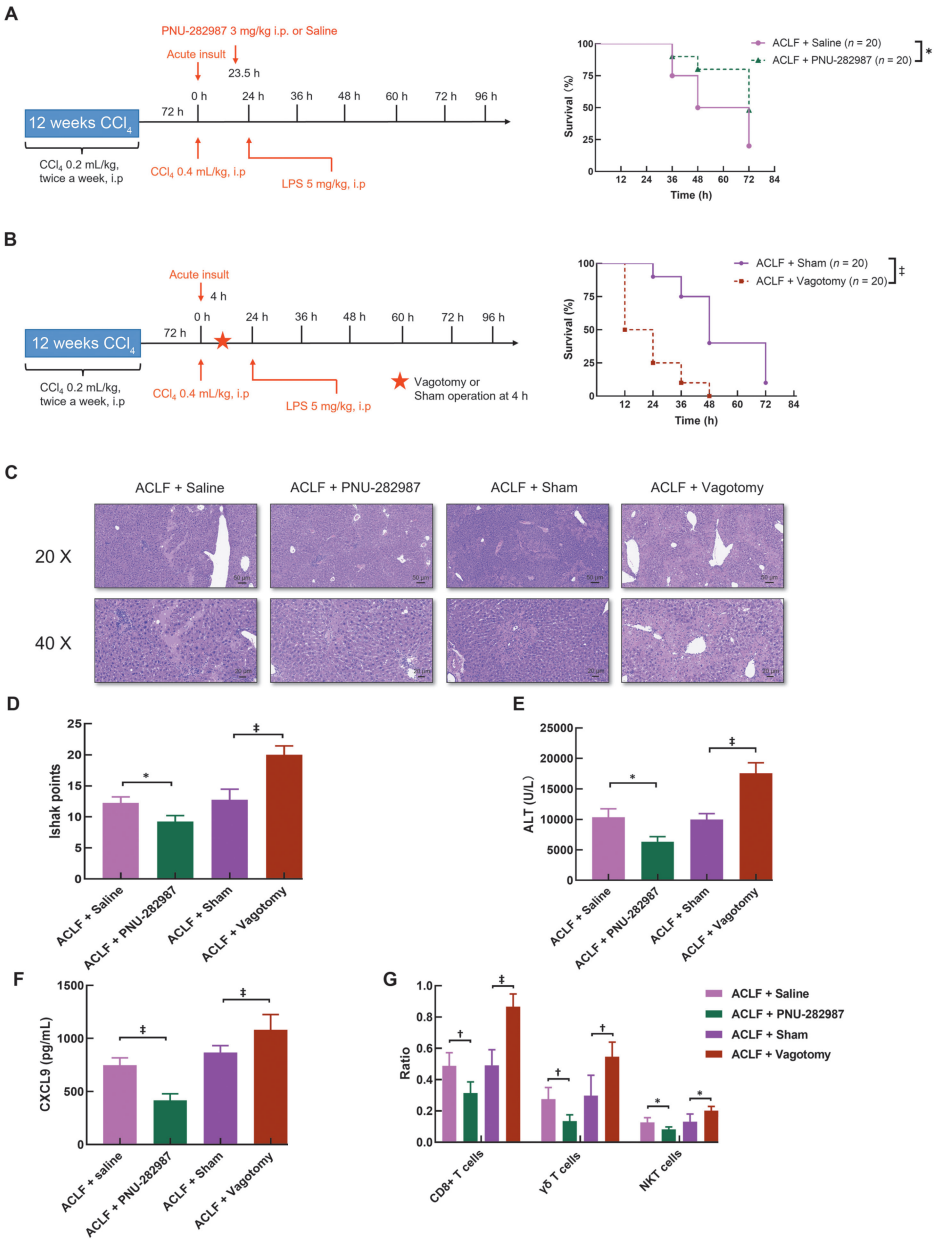

Figure 3: The vagus nerve regulated CXCL9 and the pathogenesis of ACLF. (A,B) The vagus nerve intervention experiments of ACLF mice were performed by applying PNU-282987 (a specific α7 nicotinic AChR agonist) or vagotomy operation. And mice treated with saline and sham operation were acted as control group, respectively. Survival rates were determined and Mantel-Cox log-rank test was used for statistical analysis ($n = 20$). (C) Representative hematoxylin & eosin staining images. (D, E) Comparison of Ishak points and serum ALT levels. (F) The serum CXCL9 levels were measured using enzyme-linked immunosorbent assay kit. (G) Flow cytometry analysis of $CD8^+$ T cells, γδ T cells, and NKT cells in the liver. Data were given as mean with standard deviation and *P*-values were calculated using one-way analysis of variance . $^*P < 0.05$; $^\dagger P < 0.01$; $^\ddagger P < 0.001$. AchR: Acetylcholine receptor; ACLF: Acute-on-chronic liver failure; ALT: Alanine aminotransferase; CXCL9: C-X-C motif chemokine ligand 9; CD8: Cluster of differentiation 8; LPS: Lipopolysaccharide; NKT: Natural killer T (cells).

serum ALT levels in vagotomized mice or mice treated with PNU-282987 further supported that vagus nerve stimulation ameliorated liver injury of ACLF [Figure 3D, E].

Interestingly, the cholinergic activation by PNU-282987 decreased the serum levels of CXCL9 in mice with ACLF while vagotomy did the opposite [Figure 3F]. Similar to the trend of the chemokine CXCL9, the accumulation of hepatic inflammatory cells, i.e., $CD8^+$ T cells, γδ T cells, and NKT cells, regulated by CXCL9 as mentioned above, were attenuated by PNU-282987 but aggravated by vagotomy in mice with ACLF [Figure 3G]. There was no significant difference in the percentage of $CD4^+$ T cells and neutrophils among ACLF mice with or without vagus nerve intervention [Supplementary Figure 3A,B, http://links.lww.com/CM9/B975]. The macrophages and proinflammatory M1 macrophages were decreased while the immunosuppressive M2 macrophages were increased in the liver of ACLF mice with cholinergic activation by PNU-282987 [Supplementary Figure 3C–E, http://links.lww.com/CM9/B975]. On the contrary, vagotomy obviously increased the macrophages and M1 subsets in the liver of ACLF mice compared with the sham group [Supplementary Figure 3D,E, http://links.lww.com/CM9/B975]. The $CXCR3^+CD8^+$ T cells were decreased in ACLF mice with cholinergic activation and increased in those with vagotomy [Supplementary Figure 3D, http://links.lww.com/CM9/B975]. These findings suggested that the vagus nerve modulated CXCL9/CXCR3 axis-mediated inflammatory cells' accumulation in the pathogenesis of ACLF.

To further validate the critical role of vagus nerve-mediated CXCL9 in the progression of ACLF, we observed the effect of blockage of CXCL9 as well as its receptor CXCR3 on the development of ACLF in vagotomized mice [Figure 4A]. Though the mortality of vagotomized ACLF mice with anti-CXCR3 treatment was higher compared with sham-operated ACLF mice with IgG, the mortality of mice with ACLF subjected to vagotomy was attenuated by supplementation of anti-CXCL9 or anti-CXCR3 [Figure 4A]. Meanwhile, the blockage of CXCL9 or CXCR3 also ameliorated the liver injury in mice with ACLF subjected to vagotomy, as shown by the H&E staining results and Ishak scores [Figure 4B, C]. The serum ALT levels were also decreased in vagotomized mice treated with anti-CXCL9 or anti-CXCR3 compared to those treated with IgG [Figure 4D]. Moreover, the $CD8^+$ T cells, γδ T cells, and NKT cells were accumulated in vagotomized mice and their numbers were markedly decreased after the blockage of CXCL9 or CXCR3 using neutralizing antibodies [Figure 4E]. Overall, these findings underscored the CXCL9/CXCR3 axis in mediating the modulation role of the vagus nerve in ACLF development.

Macrophages were the major source of CXCL9 in ACLF under the control of vagus nerve cholinergic signaling

To determine whether the increased CXCL9 seen in the ACLF murine model can be replicated in ACLF patients, immunohistochemical analysis of CXCL9 was performed

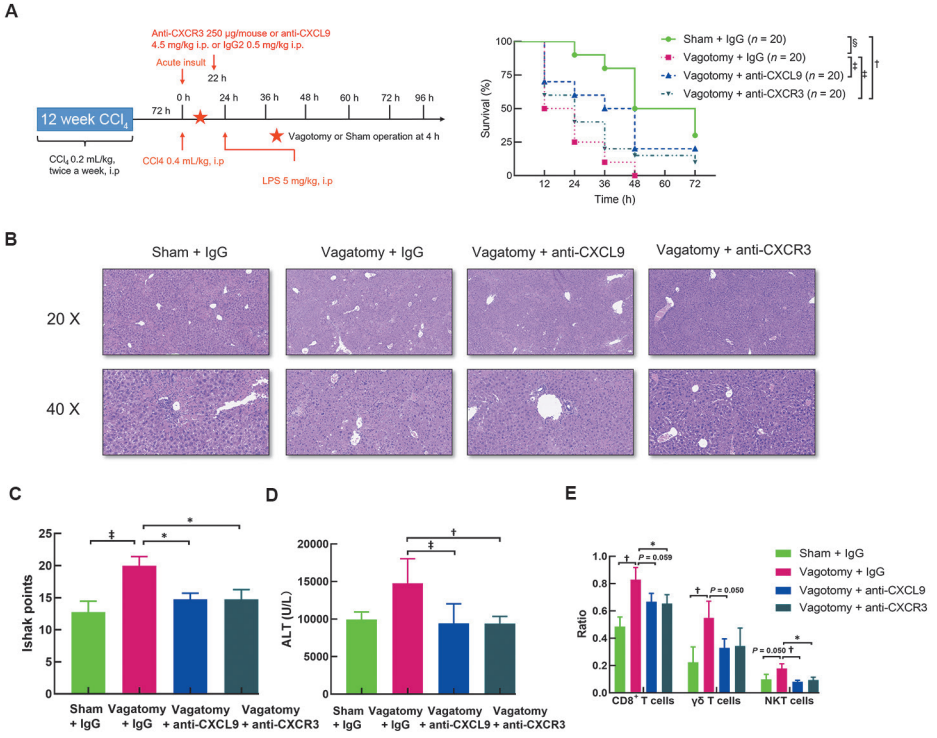

Figure 4: Supplementation with CXCL9 and CXCR3 antibodies abrogated the detrimental effect of vagotomy on ACLF pathogenesis. (A) Schematic timeline of the procedures. ACLF model mice with vagotomy operation were treated with anti-CXCL9 or anti-CXCR3 antibody. Survival rates were determined and Mantel–Cox log-rank test was used for statistical analysis ($n = 20$). (B) Representative hematoxylin & eosin staining images. (C, D) Comparison of Ishak points and serum ALT levels. (E) Flow cytometry analysis of $CD8^+$ T cells, γδ T cells, and NKT cells in the liver. Data were given as mean with standard deviation and *P*-values were calculated using one-way ANOVA. $^*P < 0.05$; $^\dagger P < 0.01$; $^\ddagger P < 0.001$. ACLF: Acute-on-chronic liver failure; ALT: Alanine aminotransferase; CXCL9: C-X-C motif chemokine ligand 9; CXCR3: C-X-C chemokine receptor 3; CD8: Cluster of differentiation 8; NKT: Natural killer T (cells); LPS: Lipopolysaccharide;

in the liver tissues from patients with ACLF and CLD. As shown in Figure 5A, the CXCL9-positive areas were markedly increased in ACLF patients compared to that in the CLD patients. Interestingly, the strong staining of CXCL9 mainly resided in cells from the portal area and cells infiltrated in the liver hepatic lobule instead of parenchyma cell as assessed by two experienced pathologists [Figure 5A]. This phenomenon suggested that CXCL9 was mainly derived from inflammatory cells instead of hepatocytes. Thus, we performed scRNA-seq to explore the immune cells responsible for the increased CXCL9 expression in the liver of ACLF. As shown in Figure 5B, C, six clusters of immune cells were identified and almost all of these cells from the liver of ACLF expressed higher levels of CXCL9 than those in the CLD mice. Remarkably, macrophages were the major producer of CXCL9 in the liver of both CLD and ACLF mice and showed increased CXCL9 expression in ACLF than in CLD [Figure 5C]. To confirm macrophages were the critical source of CXCL9, double immunofluorescence staining was conducted. The colocalization analyses of CXCL9 and F4/80 revealed that CXCL9 was predominantly expressed in the macrophages [Figure 5D]. Flow cytometry analysis further revealed that CXCL9 was predominantly expressed in the proinflammatory subtype of macrophage defined as $CD45^{+}F4/80^{+}iNOS^{+}CD206^{-}$ [Figure 5E].

Macrophages with CXCL9 depletion were produced via CRISPR/Cas9 technology and cocultured with hepatocytes. As shown in Figure 5F, the ALT levels in the supernatants from these hepatocytes were significantly decreased after LPS stimulation. In contrast, depletion of CXCL9

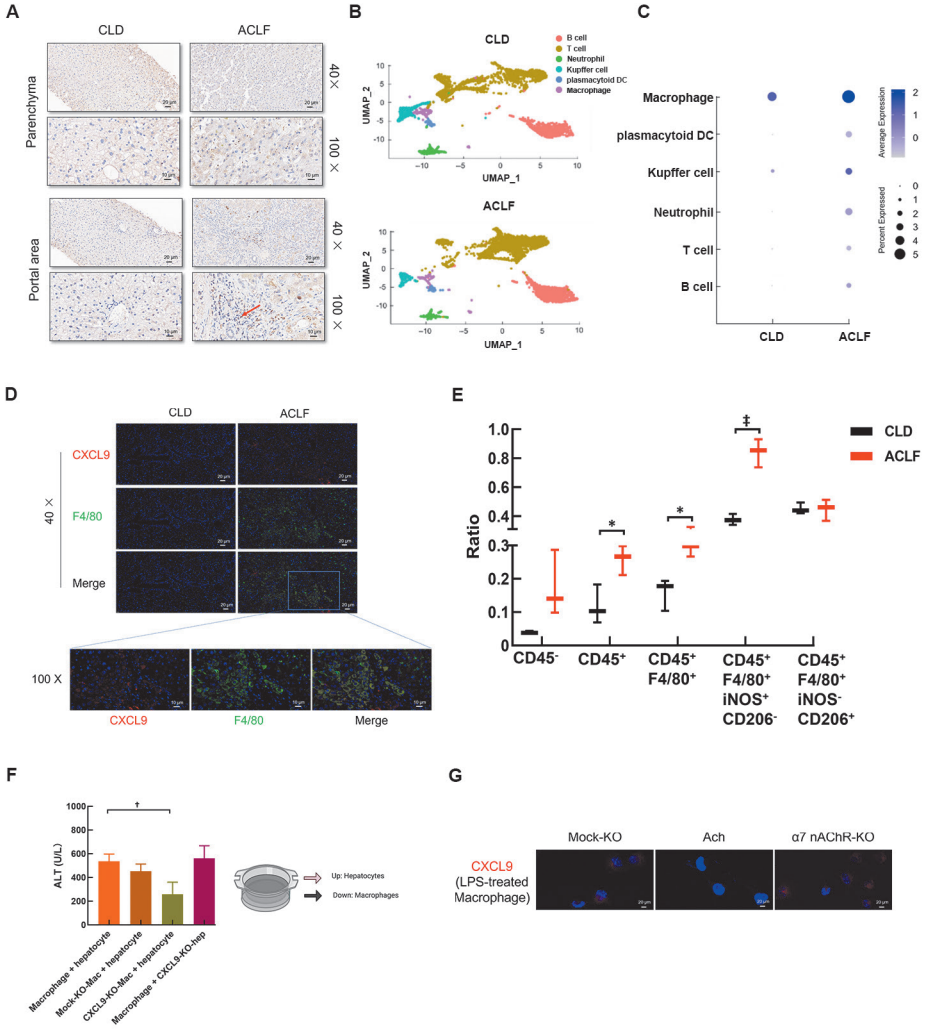

Figure 5: Macrophages were the major source of CXCL9 in ACLF. (A) Immunohistochemistry staining of CXCL9 (CXCL9-positive areas were highlighted by red arrows) in the liver tissue of CLD and ACLF patients. (B) UMAP plot showing six clusters which were identified by integrated analysis based on scRNA-seq and colored by cell cluster. (C) Bubble chart presented the expression of CXCL9 across different cell clusters. The size of the Bubble size depended on the percent of cells in a cluster expressing CXCL9, and color intensity depended on the average gene expression within a cluster. (D) Double immunofluorescence staining for CXCL9-expressing macrophage using CXCL9 (red) and F4/80 (green) in liver sections of CLD and ACLF mice. (E) The expression of CXCL9 in hepatic immune subsets of CLD and ACLF mice was determined using flow cytometry. (F) The ALT levels in the supernatant of hepatocytes and macrophages coculture system. (G) Human macrophages were treated with ACh or with genetic knockout of α7 nAChR, and Mock-KO was used as control. Then these macrophages were co-incubated with LPS for two hours and the CXCL9 concentration in supernatant was assessed using immunofluorescence staining. Data were given as median with range or mean with SD and *P*-values were calculated using one-way ANOVA or Kruskal–Wallis test. $^{*}P<0.05$; $^{\dagger}P<0.01$; $^{\ddagger}P<0.001$. α7 nAChR: α7 nicotinic acetylcholine receptor; ACh: Acetylcholine; ACLF: Acute-on-chronic liver failure; ALT: Alanine aminotransferase; CXCL9: C-X-C motif chemokine ligand 9; CLD: Chronic liver disease; LPS: Lipopolysaccharide; scRNA-seq: Single-cell RNA sequencing; SD: Standard deviation; UMAP: Uniform manifold approximation and projection; KO: Knockout.

in hepatocytes did not affect the ALT levels in the supernatants from hepatocytes cocultured with normal macrophages [Figure 5F]. Moreover, immunofluorescence analysis revealed a substantial decrease in LPS-induced CXCL9 expression in macrophages when stimulated with ACh [Figure 5G]. In contrast, the genetic knockout of α7 nicotinic AChR abrogated the inhibitory effects of ACh on CXCL9 expression in macrophages [Figure 5G], indicating vagus nerve modulates the production of CXCL9 in a α7 nicotinic AChR-dependent manner.

The DEGs of α7 nicotinic AChR-expressing cells and CXCL9-expressing macrophages were identified using scRNA-seq. Then, GO and KEGG enrichment analyses were performed to explore the biological mechanisms involved in α7 nicotinic AChR-modulated CXCL9 expression of macrophages during ACLF based on these genes. As shown in Supplementary Figures 4A and 5A, http://links.lww.com/CM9/B975, both of the upregulated DEGs of AChR-expressing liver cells and CXCL9-expressing macrophages were enriched in 20 GO terms, and the downregulated DEGs were annotated to 21 GO modules. Among which, the upregulated DEGs were specifically enriched in apoptotic process and inflammatory process such as response to cytokine, chemokine activity, chemokine-mediated signaling pathway, cellular response to IFN-γ and IL-1, and acute inflammatory response to antigenic stimulus [Supplementary Figure 4A, http://links.lww.com/CM9/B975]. The KEGG analysis showed that only the upregulated genes annotated to the mammalian target of rapamycin (mTOR) signaling pathway, ubiquitin-mediated proteolysis, natural killer cell-mediated cytotoxicity, chemokine signaling pathway, cytokine–cytokine receptor interaction [Supplementary Figure 4B, http://links.lww.com/CM9/B975]. In terms of the downregulated genes, GO and KEGG orthology (KO) modules mainly mapped to pathways including differentiation of neuron and myoblast, myelin sheath abaxonal region structure, hydrolase activity, and immunosuppressive pathways such as relaxin signaling pathway [Supplementary Figure 5A,B, http://links.lww.com/CM9/B975]. These results suggested that the pathway involved in α7 nicotinic AChR-modulated CXCL9 expression of macrophages during ACLF might relate to enhanced inflammatory response accompanied by increased apoptotic process and suppressed neuron differentiation. Taken together, these findings suggested that the CXCL9 derived from macrophage-mediated liver inflammation during ACLF progression and this process was modulated by the vagus nerve. A summary of these results is presented in a graphical abstract [Figure 6].

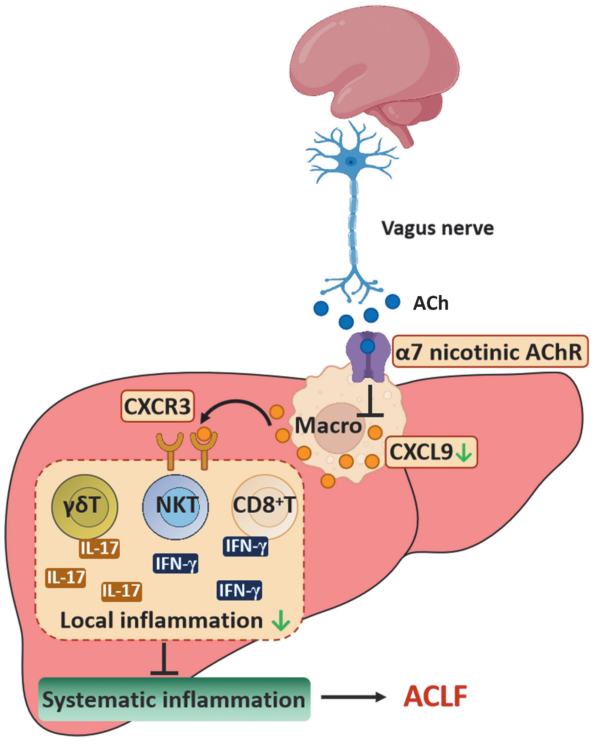

Figure 6: The vagus nerve modulates acute-on-chronic liver failure progression via CXCL9. Vagus nerve activation releases ACh to bind with α7 nicotinic AChR in macrophage which inhibited the release of CXCL9. Then, the decreased CXCL9 prevented the accumulation of CXCR3-expressing immune cells including γδ T cells, NKT cells, and $CD8^+$ T cells and the production of inflammatory cytokines of IL-17 and IFN-γ in the liver. Thus, the vagus nerve-mediated CXCL9 reduction ameliorating the local inflammation and the subsequent systemic inflammation to prevent the development of ACLF. ACh: Acetylcholine; AChR: Acetylcholine receptor; ACLF: Acute-on-chronic liver failure; CXCL9: C-X-C motif chemokine ligand 9; CXCR3: C-X-C chemokine receptor 3; CD8: Cluster of differentiation 8; IL:Interleukin; NKT: Natural killer T (cells).

Discussion

Understanding the regulatory mechanism that governs the inflammatory process is an important scientific question in the field of ACLF-associated research. In the current study, proteomic profiling results identified CXCL9 as the key molecule linked to ACLF development. Consistently, the CXCL9 expression was significantly increased in ACLF patients and was related to systematic inflammation and high mortality. Furthermore, we demonstrated that the blockade of CXCL9 attenuated liver injury and decreased the accumulation and activation of inflammatory cells in the livers of mice with ACLF. Moreover, we revealed that the increase in CXCL9 expression in ACLF derived from inflammatory macrophages, which was modulated by the vagus nerve. Notably, vagus nerve stimulation attenuated ACLF. In contrast, vagotomy aggravated liver injury in ACLF and this effect was abrogated by blocking CXCL9 and its receptor CXCR3. These findings revealed the critical role of the vagus nerve–macrophage–CXCL9 axis in the inflammatory process in ACLF, providing novel targets for treating and preventing ACLF.

In the present study, CXCL9 was identified as the major differential expressed protein in the livers from mice with ACLF compared to those with CLD. Moreover, the expression of CXCL9 gradually increased in the following order: CLD patients <ACLF-survivors <ACLF-non-survivors. Blockade of CXCL9 ameliorated liver inflammation and decreased mortality in mice with ACLF. It was reported that the principal chemokines orchestrating immune cells' migration in immune-mediated liver diseases included CXCL9, CXCL10, CXCL11, CCL20, and CXCL12.[24] Among which, only CXCL9 was increased in our ACLF patients. Previous studies have revealed increased CXCL9 levels in patients with Hepatitis B virus (HBV) infection and liver cirrhosis.[25,26]

And increased CXCL9 levels in liver cirrhosis patients receiving transjugular intrahepatic portosystemic shunt were related to refractory ascites and renal dysfunction,[26] which were risk factors for developing ACLF. These findings suggested the critical role of CXCL9 in the occurrence, development, and worsening of ACLF. As a chemokine, CXCL9 acted as a ligand for CXCR3 to recruit inflammatory cells.[24] For example, CXCL9 was reported to be involved in the hepatic migration of adaptive T lymphocytes, including Th1 and Th17 lymphocytes, into the portal vein in autoimmune liver injury.[24,27] Here, we found that in ACLF, the populations of hepatic immune cells, including $CD8^+$ T cells, innate-like T lymphocytes of NKT cells, and γδ T cells, were modulated by the CXCL9/CXCR3 axis. Unlike the adaptive T lymphocytes, the unique immunological properties of the innate-like T lymphocytes permit their participation in the early phases of immune responses in liver diseases.[28] Therefore, our findings provided important insights into the mechanisms underlying the initiation of hepatic immune responses in ACLF and highlighted specific therapeutic targets that modulate the CXCL9/CXCR3 axis would be of notable interest for ACLF treatment.

We found that vagus nerve denervation increased hepatic immune cells and mortality of mice with ACLF while vagus nerve stimulation by the α7 nicotinic AChR agonist PNU-282987 did the opposite. The liver receives the parasympathetic nerve branch of the vagus nerve and its physiological function is mediated by the innervation of the vagus nerve.[29] The hyperdynamic circulation in portal hypertensive rodents was linked to vagal neurotransmission and vagal afferent nerves.[30] Vagus stimulation by high-frequency electrical current may ameliorate portal hypertension in cirrhotic rats.[29] Additionally, previous studies have provided various evidence for the role of the vagus nerve in modulating the metabolic functions in the liver. For instance, vagal stimulation by leptin increases very-low-density lipoprotein triglyceride secretion and reduces hepatic lipid content.[31] Furthermore, hepatic branch vagotomy was reported to cause hyperglycemia.[32] Meanwhile, the vagus nerve was also shown to be involved in hepatic peroxisome proliferator-activated receptor (PPAR)-α expression and development of steatohepatitis.[33] Although the neuroimmune interactions were shown to contribute to inflammatory damage in sepsis[34] and the immune homeostasis of colitis[35] and tumor microenvironments,[7] the role of the vagus nerve in the inflammatory process of ACLF has been rarely reported. Here, our novel findings uncovered the neuroimmune communication linking the vagus nerve to the immune dysregulation of ACLF.

Furthermore, we showed that the blockade of CXCL9 and its receptor CXCR3 abrogated the vagus nerve denervation-mediated ACLF acceleration, indicating that the neuroimmune communication of the vagus nerve in ACLF depends on CXCL9. Vagus nerve stimulation has been shown to serve as a promising therapeutic strategy for treating inflammatory bowel disease,[12] *Escherichia coli* infection,[36] and pancreatitis.[6] However, the mechanisms underlying its effects are poorly understood. In fact, the vagus nerve provides a neuronal circuit called "the cholinergic anti-inflammatory pathway (CAIP)" to inhibit inflammation.[37] On the one hand, the vagal nerve regulates the number of immune cells, including invariant natural killer T (iNKT) cells, neutrophils, γδ T cells, innate lymphoid cells, and Treg cells.[34,36] On the other hand, vagal neural stimulation reduced the production of pro-inflammatory molecules and cytokines by disrupting signaling cascades, including the signal transducer and activator of transcription 3 (STAT3) signaling cascade which induces microRNA production and the activity of activating kinases.[37] In the current study, we revealed that CXCL9 was required for the vagus nerve-mediated regulation of immune responses in ACLF development. These findings highlighted the essential role of CXCL9 in interfacing with complex immune and neural communication which raising the theory of the involvement of neuroimmunoregulatory circuits in the pathogenesis of ACLF.

Moreover, we revealed that CXCL9 was derived from proinflammatory subtype of macrophage, which was modulated by vagus nerve cholinergic signaling through α7 nicotinic AChR. Although CXCL9 can be secreted by multiple cell types, it was reported that hepatic macrophages were the predominant producer.[38] Here, results from the immunohistochemical staining of ACLF samples, flow cytometry analysis and scRNA-seq in animal model, and *in vitro* experiments confirmed that macrophages were the predominant source of CXCL9 in ACLF. Macrophages have been reported to play key roles in the initiation and progression of ACLF and contribute to hepatic inflammation and subsequent systemic inflammation.[39] Identification of anti-inflammation reflexes to silence macrophage activation remains a challenge associated with ACLF treatment. Notably, we found that the CXCL9 secretion from macrophages was unregulated after α7 nicotinic AChR depletion. Similar to our findings, previous studies on lethal endotoxemia and polymicrobial sepsis showed that the vagus nerve inhibited the TNF-α production by macrophages via interactions with α7 nicotinic AChR.[18,40] Based on these findings, our results suggested that the signals transmitted through vagus nerve fibers inhibit CXCL9 production from macrophages to ameliorate liver injury and systemic inflammation in ACLF. Thus, our findings provided evidence for the therapeutic implications of neuromodulation with regard to ACLF treatment.

This study still has several limitations. First, the proteomics analysis, together with the intervention experiment in animal model, validated the key role of CXCL9 in the progression of ACLF, which were confirmed in the serum and liver samples from patients. However, further clinical validation via the analysis of more samples from ACLF patients is needed. Second, the *in vivo* and *in vitro* results evidenced that the vagus nerve regulated macrophage-derived CXCL9 release in ACLF pathogenesis. These findings need to be further examined via systematic experiments in the future to elucidate the neuroimmune communication in ACLF. This, in turn, will prompt the formulation of preclinical theories to understand the therapeutic implications of the findings reported in the present study.

In summary, our findings identified the key role of CXCL9 in mediating the immune dysregulation of ACLF and macrophage was the major source of CXCL9 which was controlled by vagus nerve cholinergic signaling. Importantly, vagus nerve stimulation attenuated liver inflammation and mortality of ACLF. Our work provided novel insights into the inflammatory process of ACLF, highlighting the neuroimmunoregulatory circuits of the vagus nerve–macrophage–CXCL9 axis contributed to ACLF development. These exciting results raised the possibility of exploiting neuromodulation as viable approaches for preventing and treating ACLF.

Acknowledgment

We would like to thank Editage (www.editage.cn) for English language editing.

Funding

This work was supported by grants from the National Natural Sciences Foundation of China (Nos. 82070613, 82370638, 82300694), the Science and Technology Innovation Program of Hunan Province (No. 2022RC1212), the Natural Science Foundation of Hunan province (Nos. 2022JJ40827, 2023JJ10095), and the Youth Science Foundation of Xiangya Hospital (No. 2022Q02).

Conflicts of interest

None.

References

1. Wu M, Wu J, Liu K, Jiang M, Xie F, Yin X, *et al*. LONP1 ameliorates liver injury and improves gluconeogenesis dysfunction in acute-on-chronic liver failure. Chin Med J 2024;137:190–199. doi: 10.1097/cm9.0000000000002969.
2. Abbas N, Rajoriya N, Elsharkawy AM, Chauhan A. Acute-on-chronic liver failure (ACLF) in 2022: Have novel treatment paradigms already arrived? Expert Rev Gastroenterol Hepatol 2022;16:639–652. doi: 10.1080/17474124.2022.2097070.
3. Hernaez R, Solà E, Moreau R, Ginès P. Acute-on-chronic liver failure: An update. Gut 2017;66:541–553. doi: 10.1136/gutjnl-2016-312670.
4. Arroyo V, Angeli P, Moreau R, Jalan R, Clària J, Trebicka J, *et al*. The systemic inflammation hypothesis: Towards a new paradigm of acute decompensation and multiorgan failure in cirrhosis. J Hepatol 2021;74:670–685. doi: 10.1016/j.jhep.2020.11.048.
5. Ocskay K, Kanjo A, Gede N, Szakács Z, Pár G, Erőss B, *et al*. Uncertainty in the impact of liver support systems in acute-on-chronic liver failure: A systematic review and network meta-analysis. Ann Intensive Care 2021;11:10. doi: 10.1186/s13613-020-00795-0.
6. Chavan SS, Pavlov VA, Tracey KJ. Mechanisms and therapeutic relevance of neuro-immune communication. Immunity 2017;46:927–942. doi: 10.1016/j.immuni.2017.06.008.
7. Renz BW, Tanaka T, Sunagawa M, Takahashi R, Jiang Z, Macchini M, *et al*. Cholinergic signaling via muscarinic receptors directly and indirectly suppresses pancreatic tumorigenesis and cancer stemness. Cancer Discov 2018;8:1458–1473. doi: 10.1158/2159-8290.cd-18-0046.
8. Xie H, Yepuri N, Meng Q, Dhawan R, Leech CA, Chepurny OG, *et al*. Therapeutic potential of α7 nicotinic acetylcholine receptor agonists to combat obesity, diabetes, and inflammation. Rev Endocr Metab Disord 2020;21:431–447. doi: 10.1007/s11154-020-09584-3.
9. Borovikova LV, Ivanova S, Zhang M, Yang H, Botchkina GI, Watkins LR, *et al*. Vagus nerve stimulation attenuates the systemic inflammatory response to endotoxin. Nature 2000;405:458–462. doi: 10.1038/35013070.
10. Li F, Chen Z, Pan Q, Fu S, Lin F, Ren H, *et al*. The protective effect of PNU-282987, a selective α7 nicotinic acetylcholine receptor agonist, on the hepatic ischemia-reperfusion injury is associated with the inhibition of high-mobility group box 1 protein expression and nuclear factor κB activation in mice. Shock 2013;39:197–203. doi: 10.1097/SHK.0b013e31827aa1f6.
11. van Westerloo DJ, Giebelen IA, Florquin S, Bruno MJ, Larosa GJ, Ulloa L, *et al*. The vagus nerve and nicotinic receptors modulate experimental pancreatitis severity in mice. Gastroenterology 2006;130:1822–1830. doi: 10.1053/j.gastro.2006.02.022.
12. de Araujo A, de Lartigue G. Non-canonical cholinergic anti-inflammatory pathway in IBD. Nat Rev Gastroenterol Hepatol 2020;17:651–652. doi: 10.1038/s41575-020-0356-y.
13. Pavlov VA, Tracey KJ. The vagus nerve and the inflammatory reflex – Linking immunity and metabolism. Nat Rev Endocrinol 2012;8:743–754. doi: 10.1038/nrendo.2012.189.
14. Pocai A, Obici S, Schwartz GJ, Rossetti L. A brain-liver circuit regulates glucose homeostasis. Cell Metab 2005;1:53–61. doi: 10.1016/j.cmet.2004.11.001.
15. Xiang X, Feng D, Hwang S, Ren T, Wang X, Trojnar E, *et al*. Interleukin-22 ameliorates acute-on-chronic liver failure by reprogramming impaired regeneration pathways in mice. J Hepatol 2020;72:736–745. doi: 10.1016/j.jhep.2019.11.013.
16. Pontes Ferreira C, Moro Cariste L, Henrique Noronha I, Fernandes Durso D, Lannes-Vieira J, Ramalho Bortoluci K, *et al*. CXCR3 chemokine receptor contributes to specific CD8+ T cell activation by pDC during infection with intracellular pathogens. PLoS Negl Trop Dis 2020;14:e0008414. doi: 10.1371/journal.pntd.0008414.
17. Lu H, Liu H, Wang J, Shen J, Weng S, Han L, *et al*. The chemokine CXCL9 exacerbates chemotherapy-induced acute intestinal damage through inhibition of mucosal restitution. J Cancer Res Clin Oncol 2015;141:983–992. doi: 10.1007/s00432-014-1869-y.
18. Hiramoto T, Chida Y, Sonoda J, Yoshihara K, Sudo N, Kubo C. The hepatic vagus nerve attenuates Fas-induced apoptosis in the mouse liver via alpha7 nicotinic acetylcholine receptor. Gastroenterology 2008;134:2122–2131. doi: 10.1053/j.gastro.2008.03.005.
19. Xu M, Kong M, Yu P, Cao Y, Liu F, Zhu B, *et al*. Acute-on-chronic liver failure defined by Asian Pacific Association for the study of the liver should include decompensated cirrhosis. Front Med (Lausanne) 2021;8:750061. doi: 10.3389/fmed.2021.750061.
20. Wu D, Zhang S, Xie Z, Chen E, Rao Q, Liu X, *et al*. Plasminogen as a prognostic biomarker for HBV-related acute-on-chronic liver failure. J Clin Invest 2020;130:2069–2080. doi: 10.1172/jci130197.
21. Denkert C, von Minckwitz G, Brase JC, Sinn BV, Gade S, Kronenwett R, *et al*. Tumor-infiltrating lymphocytes and response to neoadjuvant chemotherapy with or without carboplatin in human epidermal growth factor receptor 2-positive and triple-negative primary breast cancers. J Clin Oncol 2015;33:983–991. doi: 10.1200/jco.2014.58.1967.
22. Rose KA, Holman NS, Green AM, Andersen ME, LeCluyse EL. Co-culture of hepatocytes and Kupffer cells as an *in vitro* model of inflammation and drug-induced hepatotoxicity. J Pharm Sci 2016;105:950–964. doi: 10.1016/s0022-3549(15)00192-6.
23. Kamimura D, Tanaka Y, Hasebe R, Murakami M. Bidirectional communication between neural and immune systems. Int Immunol 2020;32:693–701. doi: 10.1093/intimm/dxz083.
24. Czaja AJ. Review article: Chemokines as orchestrators of autoimmune hepatitis and potential therapeutic targets. Aliment Pharmacol Ther 2014;40:261–279. doi: 10.1111/apt.12825.
25. Yu X, Chen Y, Cui L, Yang K, Wang X, Lei L, *et al*. CXCL8, CXCL9, CXCL10, and CXCL11 as biomarkers of liver injury caused by chronic hepatitis B. Front Microbiol 2022;13:1052917. doi: 10.3389/fmicb.2022.1052917.
26. Berres ML, Asmacher S, Lehmann J, Jansen C, Görtzen J, Klein S, *et al*. CXCL9 is a prognostic marker in patients with liver cirrhosis receiving transjugular intrahepatic portosystemic shunt. J Hepatol 2015;62:332–339. doi: 10.1016/j.jhep.2014.09.032.
27. Borchers AT, Shimoda S, Bowlus C, Keen CL, Gershwin ME. Lymphocyte recruitment and homing to the liver in primary biliary cirrhosis and primary sclerosing cholangitis. Semin Immunopathol 2009;31:309–322. doi: 10.1007/s00281-009-0167-2.
28. Wencker M, Turchinovich G, Di Marco Barros R, Deban L, Jandke A, Cope A, *et al*. Innate-like T cells straddle innate and adaptive

immunity by altering antigen-receptor responsiveness. Nat Immunol 2014;15:80–87. doi: 10.1038/ni.2773.
29. Bockx I, Verdrengh K, Vander Elst I, van Pelt J, Nevens F, Laleman W, *et al*. High-frequency vagus nerve stimulation improves portal hypertension in cirrhotic rats. Gut 2012;61:604–612. doi: 10.1136/gutjnl-2011-301396.
30. Liu H, Schuelert N, McDougall JJ, Lee SS. Central neural activation of hyperdynamic circulation in portal hypertensive rats depends on vagal afferent nerves. Gut 2008;57:966–973. doi: 10.1136/gut.2007.135020.
31. Metz M, Beghini M, Wolf P, Pfleger L, Hackl M, Bastian M, *et al*. Leptin increases hepatic triglyceride export via a vagal mechanism in humans. Cell Metab 2022;34:1719–1731.e5. doi: 10.1016/j.cmet.2022.09.020.
32. Kwon E, Joung HY, Liu SM, Chua SC Jr., Schwartz GJ, Jo YH. Optogenetic stimulation of the liver-projecting melanocortinergic pathway promotes hepatic glucose production. Nat Commun 2020;11:6295. doi: 10.1038/s41467-020-20160-w.
33. Gao X, van der Veen JN, Zhu L, Chaba T, Ordoñez M, Lingrell S, *et al*. Vagus nerve contributes to the development of steatohepatitis and obesity in phosphatidylethanolamine N-methyltransferase deficient mice. J Hepatol 2015;62:913–920. doi: 10.1016/j.jhep.2014.11.026.
34. Trakhtenberg EF, Goldberg JL. Neuroimmune communication. Science 2011;334:47–48. doi: 10.1126/science.1213099.
35. Teratani T, Mikami Y, Nakamoto N, Suzuki T, Harada Y, Okabayashi K, *et al*. The liver-brain-gut neural arc maintains the T(reg) cell niche in the gut. Nature 2020;585:591–596. doi: 10.1038/s41586-020-2425-3.
36. Dalli J, Colas RA, Arnardottir H, Serhan CN. Vagal regulation of group 3 innate lymphoid cells and the immunoresolvent PCTR1 controls infection resolution. Immunity 2017;46:92–105. doi: 10.1016/j.immuni.2016.12.009.
37. Reardon C, Murray K, Lomax AE. Neuroimmune communication in health and disease. Physiol Rev 2018;98:2287–2316. doi: 10.1152/physrev.00035.2017.
38. Yano T, Ohira M, Nakano R, Tanaka Y, Ohdan H. Hepatectomy leads to loss of TRAIL-expressing liver NK cells via downregulation of the CXCL9-CXCR3 axis in mice. PLoS One 2017;12:e0186997. doi: 10.1371/journal.pone.0186997.
39. Triantafyllou E, Woollard KJ, McPhail MJW, Antoniades CG, Possamai LA. The role of monocytes and macrophages in acute and acute-on-chronic liver failure. Front Immunol 2018;9:2948. doi: 10.3389/fimmu.2018.02948.
40. Huston JM, Ochani M, Rosas-Ballina M, Liao H, Ochani K, Pavlov VA, *et al*. Splenectomy inactivates the cholinergic antiinflammatory pathway during lethal endotoxemia and polymicrobial sepsis. J Exp Med 2006;203:1623–1628. doi: 10.1084/jem.20052362.

How to cite this article: Wu L, Li J, Zou J, Tang DL, Chen RC. Vagus nerve modulates acute-on-chronic liver failure progression via CXCL9. Chin Med J 2025;138:1103–1115. doi: 10.1097/CM9.0000000000003104